Three-Dimensional Flow Simulation of Resin Transfer Molding Utilizing Multilayered Fiber Preform

Seung Hwan Lee,[1] Mei Yang,[2] Young Seok Song,[3] Seong Yun Kim,[1] Jae Ryoun Youn[1]

[1]*Department of Materials Science and Engineering, Research Institute of Advanced Materials (RIAM), Seoul National University, Shillim-dong, Gwanak-gu, Seoul 151-744, Korea*
[2]*Central R & D Center, Dongwoo Finechem Co, Wonjung-ri, Pyeongtaek-si, Gyeonggi-do 451-822, Korea*
[3]*Department of Mechanical Engineering, Massachusetts Institute of Technology, Cambridge, Massachusetts 02139*

Received 21 January 2009; accepted 22 April 2009
DOI 10.1002/app.30698
Published online 24 June 2009 in Wiley InterScience (www.interscience.wiley.com).

ABSTRACT: Impregnation of the multi-layered fiber preform with injected resin was analyzed by using the control volume finite element method for three-dimensional mold filling simulation of the resin transfer molding (RTM). Numerically predicted flow fronts were compared with experimental data to validate accuracy of the numerical results and applicability of the numerical code developed in this study. Since isothermal Newtonian flow was assumed, Darcy's law and continuity equation were used as governing equations and permeability tensors employed for each layer. Flow simulation was conducted for the two types of mold geometries, i.e., rectangular plate and hollow cylinder. It was proven by comparing numerical results with experimental data that the simulation code is accurate enough to predict the flow patterns, especially when multi-layered preforms were placed in the cylindrical mold. It was also found that the filling time was reduced by using outer gates compared with the case of inner gates. Three-dimensional numerical simulation provided useful information for mold filling and can be used to design an optimum mold and make the RTM process efficient. © 2009 Wiley Periodicals, Inc. J Appl Polym Sci 114: 1803–1812, 2009

Key words: RTM; fiber preform; mold filling; permeability; simulation

INTRODUCTION

Liquid composite molding (LCM), which includes resin transfer molding (RTM) and vacuum assistant resin transfer molding (VARTM), has been received keen interest due to its many advantages, e.g., low equipment cost, no abrasive action of fibers against the mold surface, short cycle time compared with hand layup and filament winding, and capability of high quality. In general, it includes placing fiber preforms into a mold, compacting the preform and closing the mold, injecting resin through gates under proper pressure, and removing the final part out of the mold when the resin is cured.[1–3] RTM has gained outstanding interest in production of high-volume parts for automotive, aerospace, marine, and railroad industries. The greatest advantage of RTM is that the mechanical properties can be controlled in the most efficient way through selection of the fiber architecture and piling up of preforms in different manner. However, structure of the fiber assembly affects permeability of the preform because different fiber orientation results in different compaction behavior, which shapes the microflow channels or paths of the injected resin. Therefore, it is necessary to understand the RTM process thoroughly because the resin flow through the complicated fiber structure is complex, and the injected resin may have viscoelastic properties.[4–11]

Mold filling stage is considered as one of the most critical and complicated stages throughout the entire RTM process, and it has a great influence on the performance and quality of final parts. For multilayered preforms with multiaxial fiber structure and unique permeability tensor, it is difficult to observe the flow pattern inside the preform even with a transparent mold because preforms have intricate fiber structure and injected resin shows complex flow behavior in fiber preforms. In the mold filling stage, there are several variables for controlling complex filling pattern, e.g., injection pressure, permeability of the preform, viscosity of the resin, and mold temperature.[12,13] Flow front advancement inside fiber preforms have been observed experimentally with various methods such as radiography, electrical wires, optical fibers, ultrasound transmission, and so forth.[14–17] However, it is hard to comprehend effects of the mold filling parameters on flow front pattern during filling. Therefore, it is necessary to study

Correspondence to: J. R. Youn (jaeryoun@snu.ac.kr).
Contract grant sponsor: Korea Science and Engineering Foundation, KOSEF [Korean government (MEST)]; contract grant number: R11-2005-065.
Contract grant sponsor: Intelligent Textile System Research Center (ITRC).

interrelationship among filling parameters, flow behavior during RTM, and physical properties of final parts.

On the other hand, many numerical methods have been developed for the RTM process, e.g., finite-difference method (FDM), finite element method (FEM), boundary element method (BEM), and so forth.[18–21] Mold filling simulation has been also carried out based on these various simulation methods. However, the complexity and calculating time for simulation was significantly increased when the calculation domain and mesh should be regenerated at every time step as the flow front advances in the Lagrangian methods. Advani and Sozer[22] predicted the filling patterns for complex shell-like mold using control volume finite element method since the mesh regeneration for filling simulation of complex mold geometry can be done with CVFEM efficiently. Cho et al.[23] and Seong et al.[24] investigated the permeability in the in-plane and transverse directions experimentally and predicted flow patterns within multi-layered fiber preforms in a unidirectional flow. Song[25] also examined the in-plane and transverse permeabilities of preforms based on the structure of various fiber mats and fabrics. However, there are few reports on practical applications to resin transfer molding although three-dimensional numerical simulation has been proved to be a useful tool for prediction of the resin flow in injection molding.[14,26–28]

It is well known that a transparent mold and a CCD camera have been used to understand the flow front advancement with respect to time during filling of the mold. Although the transparent mold experiments allow flow observation only for surface and edge of preforms, it has been known that they offer satisfactory results for validation of simulation results.[23,29] In this study, three-dimensional mold filling simulation of RTM was used to investigate the flow pattern in multi-layered and cylindrical braided fiber preforms since the flow pattern could not be observed by experimental method precisely. To validate the simulation results, experimental observation was also conducted in both radial and transverse directions. Experimentally observed flow front patterns were compared with numerical results. All permeabilities used in mold filling simulation were obtained through experimental measurements so that the simulation conditions are similar to real situation. Pressure field and filling time were also calculated with given constant pressure and permeability at every time step.

THEORY

Control volume finite element method (CVFEM) was used to calculate velocity field in the flow domain changing continuously. The mold cavity was divided into a three-dimensional mesh by using tetrahedral elements because they are convenient for mesh generation of complicated geometries. Darcy's law and continuity equation for a control volume are given by the following equations.[23–25]

$$\text{Darcy's law}: \quad \tilde{v} = -\frac{K}{\eta}\nabla P \tag{1}$$

$$\text{Continuity equation}: \quad \nabla \cdot \tilde{v} = 0 \tag{2}$$

where $\tilde{v}$ is Darcy's velocity vector, η is Newtonian viscosity of the fluid, $\bigtriangledown P$ is pressure gradient vector, and K is permeability tensor of the porous fiber medium. Interpolation function for pressure is cast as below.

$$\int_{CV} \nabla \cdot \tilde{v} dV = 0$$
$$\int_{CV} \nabla \cdot \tilde{v} dV = \int_{CS} \tilde{v} \cdot \tilde{n} d\Gamma = \int_{CS} -\frac{1}{\mu} K \nabla P \cdot \tilde{n} d\Gamma = \sum_{CS} -\frac{1}{\mu} K \nabla P \cdot \tilde{n} A_i \tag{3}$$

$$P = ax + by + cz + d = N_1P_1 + N_2P_2 + N_3P_3 + N_4P_4 \tag{4}$$

To solve the flow field in a concentric cylindrical mold cavity, permeabilities measured in Cartesian coordinate system should be transformed into cylindrical coordinate system because they are measured in a rectangular mold. It was assumed that permeabilities in both radial and axial directions were the same when the fiber preforms were placed into a cylindrical cavity, as shown in Figure 1, where K_{trans} and K_{radial} were transverse and in-plane permeabilities of the fiber preform obtained experimentally, respectively. As shown in the following equation, K_r, K_θ, and K_z were obtained from experiments and then transformed into Cartesian coordinate system by the eq. (5).

$$K_r = K_{tr}$$
$$K_\theta = K_{radial}$$
$$K_z = K_{radial}$$

$$[\mathrm{K}] = \begin{bmatrix} K_{xx} & K_{xy} & K_{xz} \\ K_{yx} & K_{yy} & K_{yz} \\ K_{zx} & K_{zy} & K_{zz} \end{bmatrix}$$
$$= \begin{bmatrix} K_r\cos^2\theta + K_\theta\sin^2\theta & \sin\theta\cos\theta(-K_r + K_\theta) & 0 \\ \sin\theta\cos\theta(-K_r + K_\theta) & K_\theta\cos^2\theta + K_r\sin^2\theta & 0 \\ 0 & 0 & K_z \end{bmatrix} \tag{5}$$

I-DEAS software was used to generate the mesh for the mold cavity, and proper boundary conditions

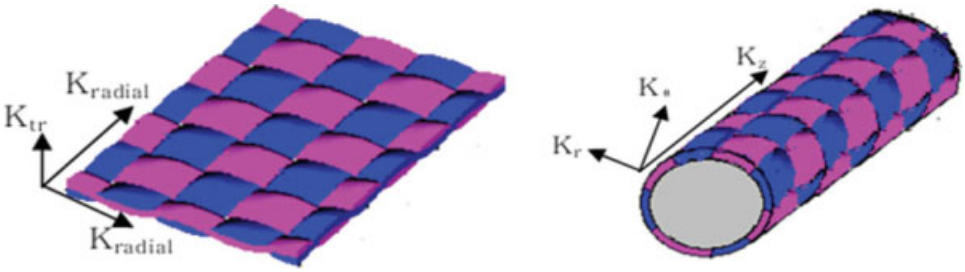

Figure 1 Transformation of the permeability tensor. [Color figure can be viewed in the online issue, which is available at www.interscience.wiley.com.]

were imposed on the boundary nodes. Pressure at every node was calculated through eq. (3) with the following boundary conditions.

$$\begin{aligned} \text{At the mold wall :} \quad & \frac{\partial P}{\partial n} = 0 \\ \text{At the injection gate :} \quad & P = P_0 \\ \text{At the flow front :} \quad & P = 0 \end{aligned} \tag{6}$$

It is well known that reduced number of linear systems is to be solved in the implicit time algorithm. In the explicit method, the pressure field is updated whenever a node is saturated. Therefore, a model with N initially unsaturated nodes will require the solution of N set of linear equations if there is no symmetry in the pressure field system.[30–34] In this study, each node was initialized in the calculation domain, and fluid velocity was obtained in every element with the known pressure field. Fill factor was introduced to determine whether the control volume is filled or not. If it is smaller than 1, the control volume is not filled, and then the control volume is filled until the fill factor is equal to 1. Status of the control volume is directly determined according to the following conditions. Time step was determined by identifying the control volume with the smallest filling time and computing the time needed to fill the control volume located at the flow front. The flow calculation domain was newly determined after each time step. The neighboring control volumes around the newly filled control volume were identified whenever one control volume is filled out. Among the neighboring control volumes, some were in the calculation domain with the fill factor of $f = 1$, some were located at the flow front with the fill factor of $0 < f < 1$, and the others were newly involved control volumes with the fill factor of $f = 0$. These newly involved nodes were added into flow front nodes and then the flow front was updated. The same calculation routine was repeated until all the control volumes were filled out ($f = 1$).

In every time step, it was assumed that the variables in the calculating domain were in steady state although mold filling was a transient problem. Therefore, it is essential to decide the accurate time step for numerical simulation of the mold filling stage. Before computing the time step, flow front nodes in the control volume were determined in advance. There are two methods to calculate the time step as shown in Figure 2. One is to compute the Δt over the entire flow front control volumes (FFCV) as below.

$$\Delta t_i = \frac{V_i}{Q_i} \tag{7}$$

where i is the FFCV index, V_i is the volume of the i-th FFCV, and Q_i is the flow rate in the i-th FFCV. Then, the control volume with minimum Δt is filled up, and the minimum value of Δt is chosen as the next time step. The other is to calculate the fill factor, f, in every time step and obtain Δt by the following equations.

$$f_i^m = f_i^{m-1} + \frac{Q_i^m t^m}{V_i} \tag{8}$$

$$\Delta t_i^m = \frac{(1 - f_i^{m-1})V_i}{Q_i^m} \tag{9}$$

where m is the time step index. The other FFCVs are partially filled at the same time when a control volume is filled up as shown in Figure 2. When the next time step starts, the partially filled FFCVs will not be empty, but it is filled up continuously from the last time step. Filling time for a rectangular mold was predicted to be 27.5 sec by using the latter method, and filling time determined experimentally was 28.5 sec.

EXPERIMENTAL

Materials and experimental set-up

Dimethyl siloxane polymer (DC 200F/100CS, Dow Corning Co.) was employed as the impregnating

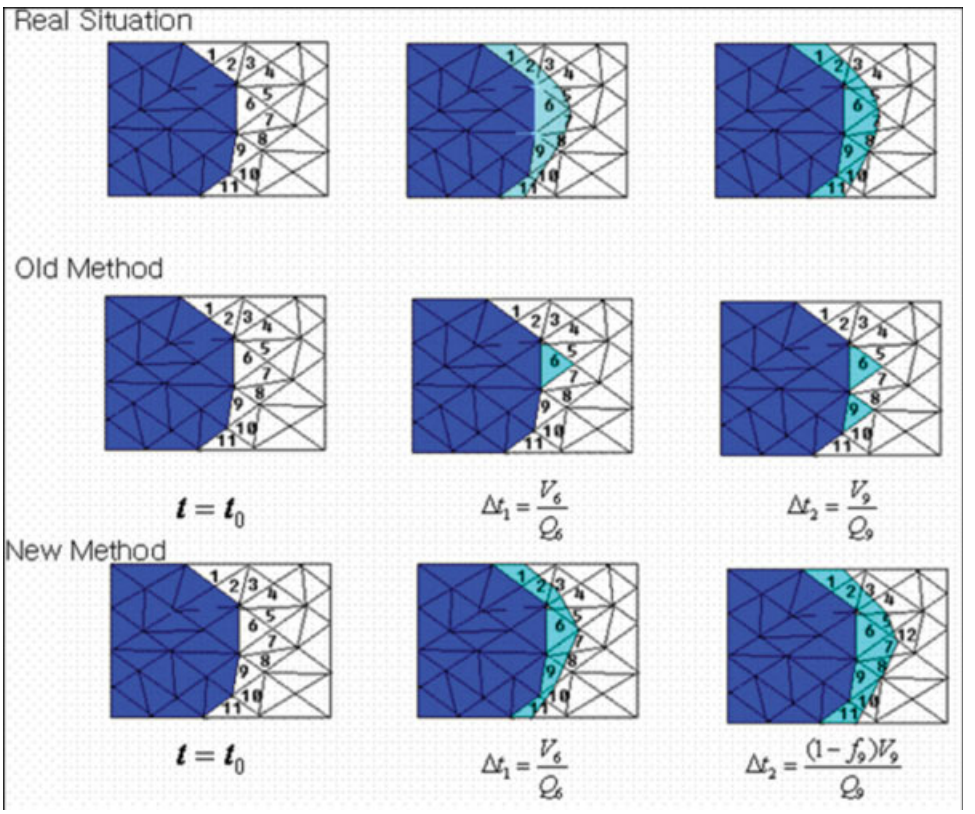

Figure 2 Two methods for calculation of time step. [Color figure can be viewed in the online issue, which is available at www.interscience.wiley.com.]

resin in this study, and the viscosity was 9.7×10^{-2} Pa · s. Plain glass fiber woven fabrics and glass fiber random mats had isotropic in-plane permeabilities due to the internal structure as shown in Figure 3(a,b). Three-dimensional braided glass fiber preform had anisotropic permeability as shown in Figure 3(c). To measure the in-plane and transverse permeabilities of fiber preforms and to validate the simulation results, several experiments were carried out in the rectangular and cylindrical molds as shown in Figure 4. The rectangular mold was composed of a base plate, an upper transparent plate, and a rectangular rim to assemble the upper plate with the base plate. By altering the distance between the two plates, height of the mold was adjusted to control the porosity of fiber preforms. Under constant pressure, the resin was injected into the cavity through a gate on the center of the base plate and then discharged through each venting hole at four corners of the base plate. The dimension of the plate was 500×500 mm^2, and the fiber preforms were cut to the size of 450×450 mm^2. CCD video camera was suspended over the transparent plate to record the flow patterns during mold filling. Radial in-

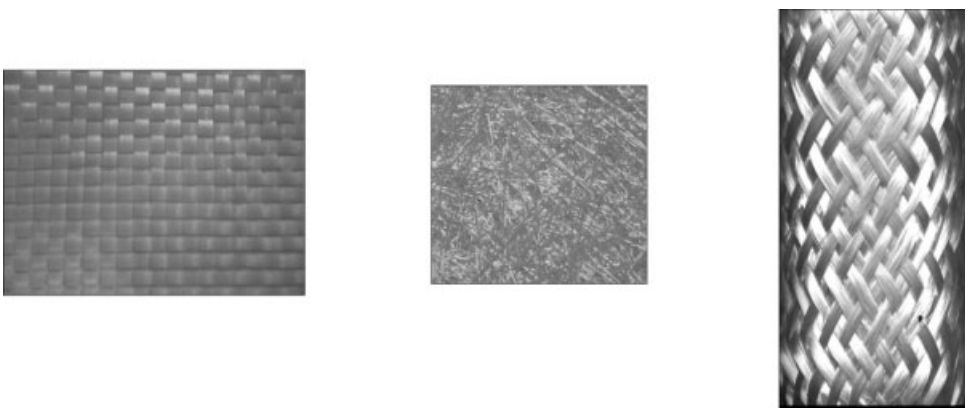

Figure 3 (a) glass fiber woven fabric, (b) glass fiber random mat, and (c) circular braided glass fibers used in this study.

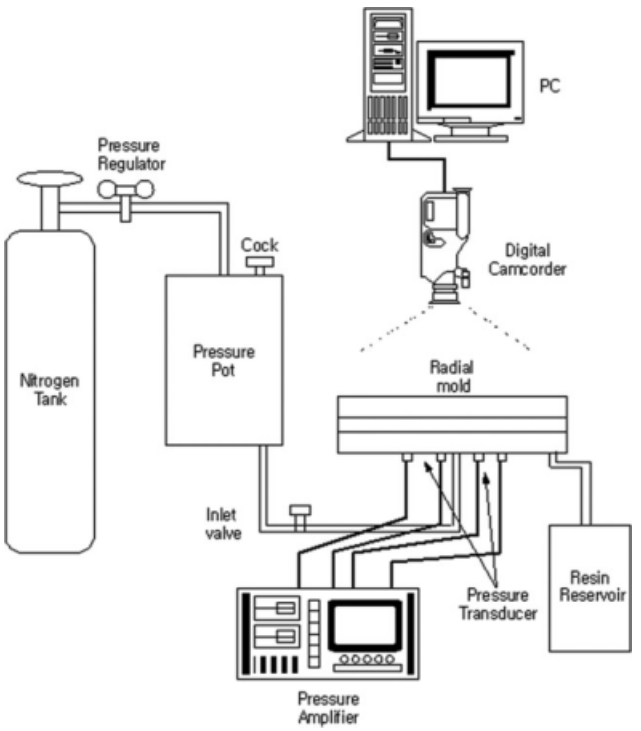

Figure 4 Schematic diagram of radial flow experimental set-up.

plane permeabilities were determined by the pressure data measured with respect to time which was recorded by Dasylab software (National Instrument Co.). Without observation of the flow front in the barrel, transverse permeability was measured by the flow rate and the pressure data. In this study, gravity effects were ignored because they are not significant in the measurement.

Permeability measurement

To measure the radial in-plane permeability, experiments were carried out by injecting the resin to the center of a fiber mat and observing a circular or elliptical flow front advancement. Two in-plane permeabilities were determined from an experimental set-up by identifying the flow front position in each principal direction. eqs. (10) and (11) were obtained by integrating eq. (1) for the entire flow domain.

$$G(\rho_x) = \frac{2\rho_x^2 \ln \rho_x - \rho_x^2 + 1}{4} = -\frac{K_{xx} P_0}{\eta x_0^2} t \tag{10}$$

$$G(\rho_y) = \frac{2\rho_y^2 \ln \rho_y - \rho_y^2 + 1}{4} = -\frac{K_{yy} P_0}{\eta y_0^2} t \tag{11}$$

where $\rho_x = x_f/x_0$, $\rho_y = y_f/y_0$ and x_f and y_f were the flow front positions in x and y directions, respectively. $G(\rho_x)$ and $G(\rho_y)$ were obtained as a function of time from experimental data. Permeability in each direction was calculated by the following equations to find the slopes of l_x and l_y with the least square method.

$$K_{xx} = -\frac{\eta x_0^2}{P_0} l_x \tag{12}$$

$$K_{yy} = -\frac{\eta y_0^2}{P_0} l_y \tag{13}$$

In the case of transverse isotropic preform, K_{xx} and K_{yy} were calculated simultaneously from the experimental data because they had the same value. For braided preform, however, they were computed separately by using eqs. (12) and (13). In-plane permeabilities of several fiber mats are shown in Table I.

To measure the transverse permeability, injection pressure and flow rate were obtained at steady state. Mold geometry used for measurement of the transverse permeability is shown in Figure 5, and flow rate in the thickness direction is given as below.

$$Q = -\frac{K_{\text{tr}}}{\eta}\frac{\partial P}{\partial z} A = -\frac{K_{\text{tr}}}{\eta}\frac{\Delta P}{\Delta z} A \tag{14}$$

where A is the area of cross section, ΔP is pressure drop, and Δz is distance. By applying eq. (14) to two permeable walls and a perform layer, the flow rate is expressed by

$$Q = -\frac{K_w}{\eta}\frac{\Delta P_w}{l_w} A = -\frac{K_{\text{tr}}}{\eta}\frac{\Delta P_p}{l_p} A = -\frac{K_t}{\eta}\frac{\Delta P_t}{l_t} A \tag{15}$$

where K_w and K_{tr} are the permeability of porous wall and fiber preform. ΔP_w is pressure drop across the mold wall with thickness l_w, and ΔP_p is pressure

TABLE I
Porosity and In-plane Permeability Measured by Experiments for Glass Fiber Woven Fabrics, Aramid Fiber Woven Fabrics, and Braided Glass Fibers

Glass fiber woven fabrics		Aramid fiber woven fabrics		Braided glass fibers	
Porosity	In-plane permeability ($\times 10^{-9}$ m^{-2})	Porosity	In-plane permeability ($\times 10^{-9}$ m^{-2})	Porosity	In-plane permeability ($\times 10^{-9}$ m^{-2})
0.42	12.1	0.44	1.23	0.66	5.547 (axial direction)
0.53	15.6	0.51	1.55		1.073 (tangential direction)
0.6	20.3	0.58	9.01		

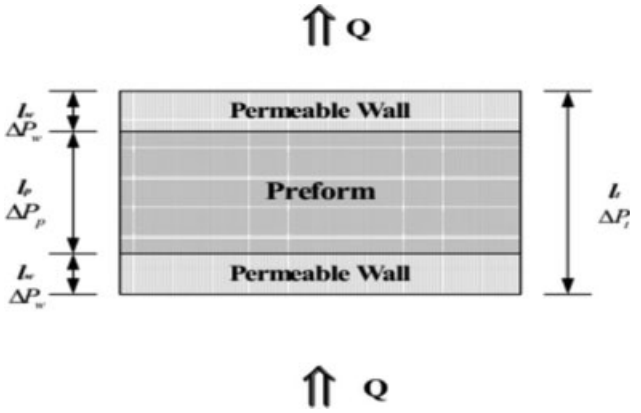

Figure 5 Schematic diagram for calculation of transverse permeability.

drop across the fiber preform with height l_p. The total pressure drop is given by

$$\Delta P_t = 2\Delta P_w + \Delta P_p \tag{16}$$

where ΔP_t is total pressure drop through the mold cavity. Equation (17) is derived by eqs. (15) and (16).

$$\frac{Q\eta}{K_t}\frac{l_t}{A} = 2\frac{Q\eta}{K_w}\frac{l_w}{A} + \frac{Q\eta}{K_{\mathrm{tr}}}\frac{l_p}{A} \tag{17}$$

Equation (18) is obtained subsequently.

$$\frac{l_t}{K_t} = 2\frac{l_w}{K_w} + \frac{l_p}{K_{\mathrm{tr}}} \tag{18}$$

In steady state flow, ΔP_t and Q were measured directly and then the total permeability K_t was computed by eq. (14) since A, l_t, and η were known beforehand. Permeability of the solid wall, K_{yy}, was determined from pressure drop (ΔP_t) and flow rate (Q) measured by letting the resin flow through two permeable mold walls without the preform. K_{tr} was calculated by eq. (18) with measured K_t and K_{yy}. The measured transverse permeabilities for different performs are shown in Table II.

Compaction test

When multi-layered preforms are used, thickness of the entire multi-layered preforms can be controlled. For calculation of porosity of each layer, it is necessary to know the thickness of each preform layer. Relationship between thickness and pressure can be known as follows by a compaction test.

$$P_g = f_g(h_g) \tag{19}$$

$$P_a = f_a(h_a) \tag{20}$$

where P_g and P_a are pressures applied to the glass fiber woven fabrics and aramid fiber woven fabrics in the compaction test. Also, h_g and h_a are thicknesses of 10 layers composed of glass and aramid fiber woven fabrics, respectively. f_g and f_a are functions which are obtained by fitting experimental data. Pressure imposed on each layer is the same in the multilayered perform and the following equation is valid.

$$f_g(h_g) = f_a(h_a) \tag{21}$$

Total thickness of the multi-layered fiber preform, H, was determined experimentally by the mold filling test.

$$\frac{n_g}{10}h_g + \frac{n_a}{10}h_a = H \tag{22}$$

h_g and h_a were obtained by eqs. (21) and (22) and then the porosity of each layer was computed by the equation below.

$$\varepsilon = 1 - \frac{\overline{m}/\rho}{l^2 h} \tag{23}$$

where $\overline{m}$ is the average mass of one layer, ρ is the fiber density, and h is the thickness calculated by using eqs. (21) and (22).

The compaction test was carried out by using the apparatus shown in Figure 6. Position of the top plate and applied force were recorded by a computer. Both glass and aramid fiber woven fabrics composed of 10 layers were used to conduct the compaction test. The fiber mat was cut into a square plate of 100 × 100 mm^2. Experimental data of the compaction test were fitted to the curve expressed as below.

$$P_g = 3.1548\exp(-3.6609h_g) \tag{24}$$

$$P_a = 1.9328\exp(-5.0373h_a) \tag{25}$$

TABLE II
Porosity and Transverse Permeability Measured by Experiments for Glass Fiber Woven Fabrics, Aramid Fiber Woven Fabrics, and Braided Glass Fibers

Glass fiber woven fabric		Aramid fiber woven fabric		Braided glass fibers	
Porosity	Transverse permeability ($\times 10^{-11}$ m^{-2})	Porosity	Transverse permeability ($\times 10^{-11}$ m^{-2})	Porosity	Transverse permeability ($\times 10^{-11}$ m^{-2})
0.55	0.50	0.50	0.18	0.66	5.6
0.60	0.69	0.55	0.23		
0.65	1.12	0.60	0.33		

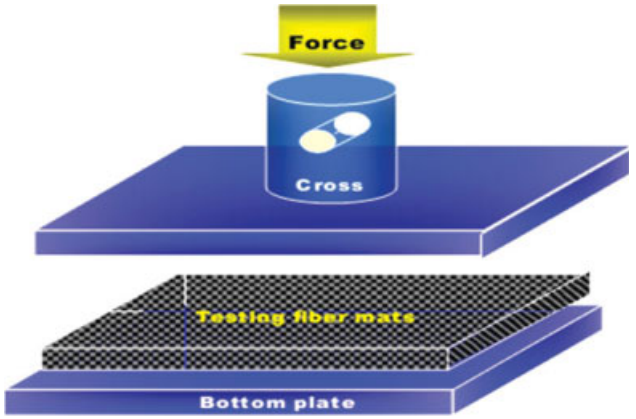

Figure 6 Schematic diagram of the experimental apparatus used in this study for compaction test. [Color figure can be viewed in the online issue, which is available at www.interscience.wiley.com.]

The total thickness of multilayered fiber preforms used in the rectangular mold filling experiment was 1.8 mm. By using eqs. (20) and (21), thickness of a glass fiber woven fabric layer was determined to be 0.32 mm and that of two aramid fiber woven fabric layers was 0.45 mm at the top and bottom of preform. Porosity of a woven glass fiber mat in the multilayered preform was 0.27 and that of an aramid fiber woven fabric mat was 0.54, which made the overall porosity 0.4.

RESULTS AND DISCUSSION

Single layer of glass fiber woven fabric

Single layer of glass fiber woven fabric was chosen for verification of the simulation code, and the porosity was set to be 0.53 by controlling the height of the rectangular mold. The mold geometry was 450 × 450 × 0.5 mm^3 with a rectangular hole at the center and the eight nodes at the hole were set to be filled at the beginning of the numerical simulation. FEM mesh and the rectangular hole are shown in Figure 7(a) and 6993 nodes and 21,136 elements were used for flow simulation of the rectangular cavity with one layer of glass fiber woven fabric. It was found by comparison with the experimental data that simulation results were accurate enough to predict the flow patterns. As shown in Figure 7(b), filling time increases exponentially in the case of rectangular mold cavity filled with one layer of glass fiber woven fabric. Although predicted data gave slightly different values for initial filling steps, they were in a good agreement with experimental data.

Multi-layered fiber preforms

To validate the numerical simulation code for more complex situation, multi-layered fiber preforms were chosen, e.g, aramid and glass fiber woven fabrics. The upper and bottom layers were made out of aramid fiber woven fabrics, and their thickness was 0.45 mm. In-plane and transverse permeabilities of the transverse isotropic aramid fiber woven fabric were measured to be 2.5 × 10^{-9} mm^2 and 2.2 × 10^{-12} mm^2, respectively. The middle layer was glass fiber woven fabric, and its thickness was 0.32 mm. In-plane and transvers permeabilities of the glass fiber woven fabric were 1.05 × 10^{-8} mm^2 and 3.6 × 10^{-12} mm^2. The whole cavity was 450 × 450 × 1.22 mm^3 and porosity of the entire preform was set to be 0.4. The thickness of each layer was calculated by

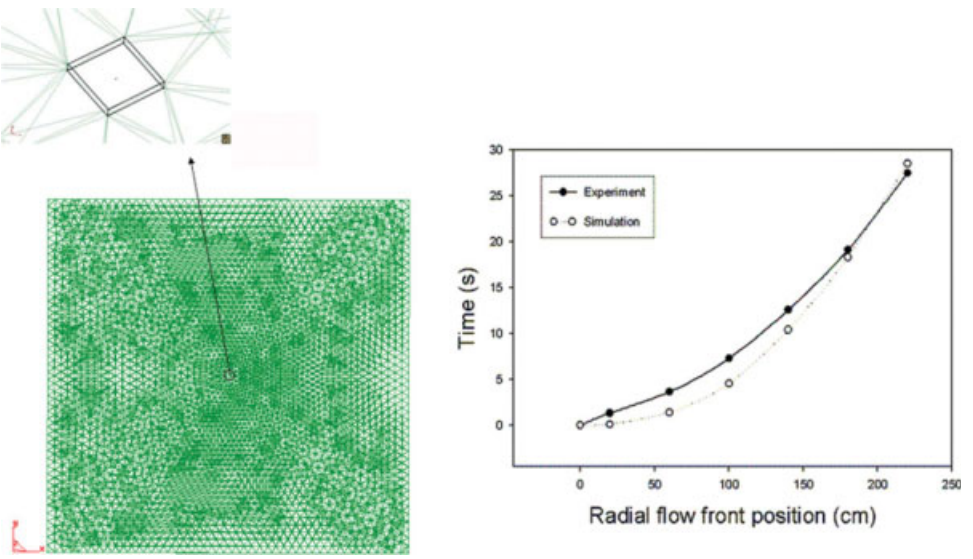

Figure 7 (a) Mesh used for flow simulation and (b) flow front reaching time for positions in rectangular mold cavity filled with one layer of glass fiber woven fabric. [Color figure can be viewed in the online issue, which is available at www.interscience.wiley.com.]

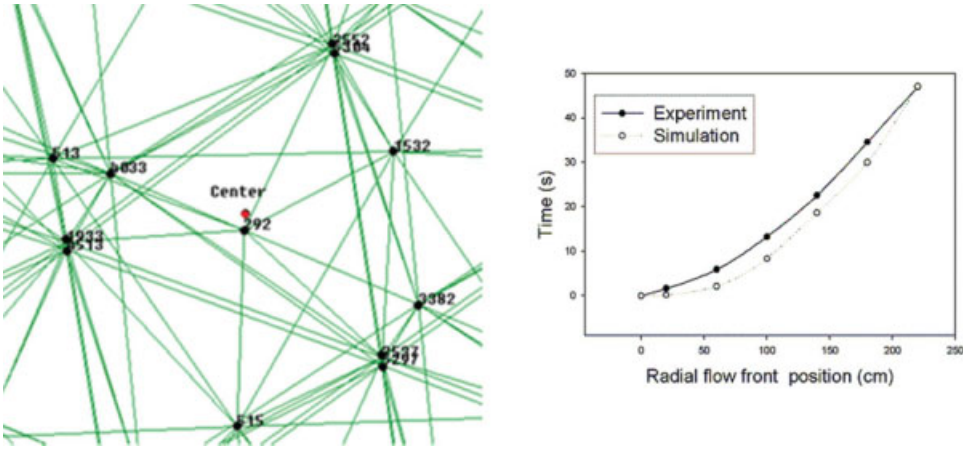

Figure 8 (a) Mesh used for flow simulation and (b) flow front reaching time for positions in rectangular mold cavity filled with multi-layered preforms. [Color figure can be viewed in the online issue, which is available at www.interscience.wiley.com.]

eqs. (21) and (22). Gate position for flow simulation in the rectangular mold cavity filled with the multi-layered preform is shown in Figure 8(a). The gate consists of the nearest 12 nodes to the center and 5588 nodes and 23,547 elements were adopted in the calculation. Numerical results calculated for filling of the rectangular mold cavity containing the multi-layered fiber preforms were compared with experimental data as shown in Figure 8(b). Filling time at the same flow front position of the top layer was compared as shown in the figure, and the simulation results were in a good agreement with experimental data. It is expected that the numerical code used in this study can be used to predict flow front advancements which cannot be observed easily by experiments.

Flow in a cylindrical mold cavity

The glass fiber braided preform used in this study for the analysis of mold filling in cylindrical mold was shown in Figure 3(c). In this case, 3993 nodes and 16,047 elements were utilized in the FEM mesh. As listed in Table I, the axial permeability was 5.547×10^{-9} m^2, the radial permeability was 5.6×10^{-11} m^2, and the tangential permeability was 1.073×10^{-10} m^2. Three permeability values were measured by experiments when the porosity is 0.66. The injection pressure was 35,000 Pa, and inner gates were employed. Pressure profiles and the flow front contours in the cylinderical mold cavity filled with braided glass fiber preforms are shown in Figure 9(a,b), respectively. The filling time was computed to be 1669 seconds. To optimize the gate positions, two cases, i.e., inner and outer gates were compared in the simulation. Figure 10(a,b) shows the different flow fronts for inner and outer gate cases at the same filling time of 1545 seconds, respectively. The black regions express the unfilled portion of the cylindrical mold. As shown in Figure 10, flow advancement is faster in the case of inner gates than in the case of outer gates.

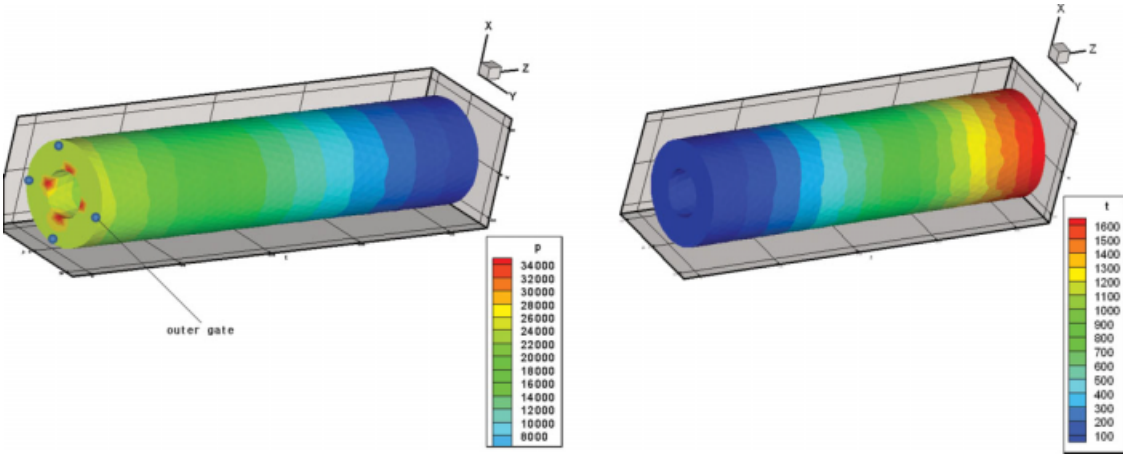

Figure 9 (a) Predicted pressure profile and (b) flow front advancement time in the cylindrical mold cavity filled with braided glass fiber preform when the cavity is filled out. [Color figure can be viewed in the online issue, which is available at www.interscience.wiley.com.]

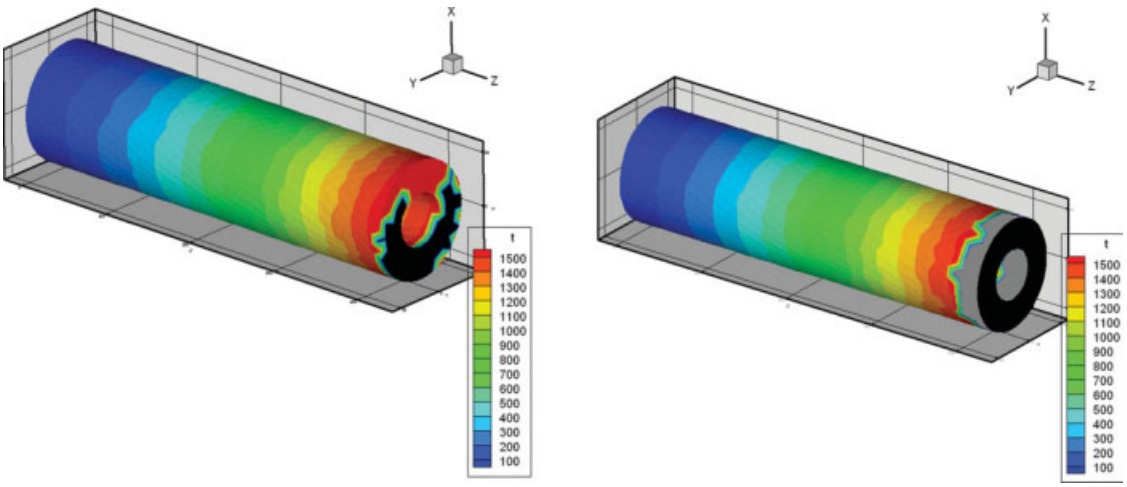

Figure 10 Flow advancement with respect to time in the case of (a) outer and (b) inner gates. [Color figure can be viewed in the online issue, which is available at www.interscience.wiley.com.]

The same FEM mesh which contains 3993 nodes and 16,047 elements was used for the simulation of cylindrical mold filled with braided preforms. The middle layer was the glass woven fabric, whose in-plane and transverse permeabilities were 2.03×10^{-8} m^2 and 6.9×10^{-12} m^2. The inner and out layers were aramid woven fabrics, in-plane permeability of which was 9.01×10^{-9} m^2 and transverse permeability was 3.3×10^{-12} m^2. These permeabilities were measured in a rectangular mold. Three layers had the same thickness of 10 mm and injection pressure used in this study was 100,000 Pa. Figure 11 shows predicted flow front advancement and the pressure profile in the multi-layered preform. As expected, the resin flows faster in the middle layer than in both inner and outer layers, but the difference is not significant. The flow prediction is compared with the results of the experimental studies reported previously, and there is a good agreement.[23–25] When constant pressure is applied at the inlet, the pressure gradient becomes smaller as the flow front progresses. The flow front moves fast at initial stage but its velocity becomes slower since the flow reaches steady state as flow front progresses. The numerical results predicted by using the three-dimensional simulation code developed in this study were in a good agreement with experimental results in the case of both rectangular and cylindrical geometry cavities. This was attributied to accurate measurement of permiablities of various fiber preforms as well as proper assumptions and governing equations applied to the numerical simulation.[35–40] Since the newly developed code in this study was based on CVFEM method which can regenerate FEM mesh efficiently, complexity and calculation time for simulation could be reduced sufficiently by using the code. Therefore, it is expected that the numerical code will contribute to studies on mold filling similation of RTM which can not be visualized by experiments.

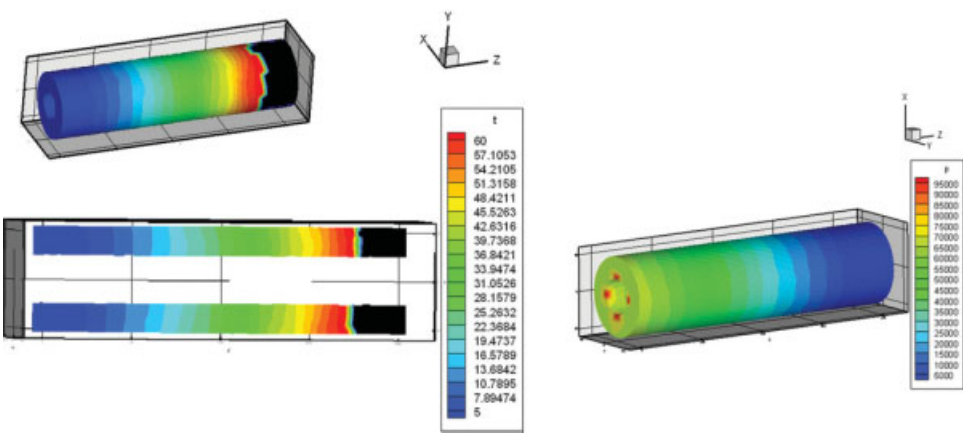

Figure 11 (a) Predicted flow front profile and (b) pressure contours in cylindrical mold cavity filled with multi-layered preforms. [Color figure can be viewed in the online issue, which is available at www.interscience.wiley.com.]

CONCLUSIONS

Three-dimensional mold filling simulation of RTM was performed numerically by using time step calculation method. Experiments were carried out to measure the permeability of various fiber preforms, and the permeability values were used as the input parameter for numerical simulation. A CVFEM code was developed to regenerate FEM mesh efficiently and reduce calculation time for simulation. When compared with the experimental data, simulation results were useful for prediction of the flow patterns. The simulation results were also in good agreement with experimental data for filling time at the same flow front position. It was found by the predicted flow patterns in the cylindrical mold filled with various braided fiber preforms that using outer gates reduced the filling time compared with the case of inner gates. The three-dimensional numerical simulation provided useful information for mold filling process and can be used for design of an optimum mold and efficient RTM process.

References

1. Harper, C. A. Handbook of Plastic Processes; Wiley-Interscience: Hoboken, 2006.
2. Long, A. C. Design and Manufacture of Textile Composites; CRC Press: Boca Raton, 2005.
3. Song, Y. S.; Youn, J. R. Polym Composite 2008, 29, 390.
4. Cecen, V.; Seki, Y.; Sarikanat, M.; Tavman, I. H. J Appl Polym Sci 2008, 108, 2163.
5. Advani, S. G.; Sozer, E. M. Process Modeling in Composites Manufacturing; CRC Press: Boca Raton, 2002;
6. Sreekumar, P. A.; Albert, P.; Unnikrishnan, G.; Joseph, K.; Thomas, S. J Appl Polym Sci 2008, 109, 1545.
7. Bhat, P.; Merotte, J.; Simacek, P.; Advani, S. G. Compos Part A – Appl S 2009, 40, 431.
8. Simacek, P.; Advani, S. G.; Iobst, S. A. J Compos Mater 2008, 42, 2523.
9. Kelly, P. A.; Umer, R.; Bickerton, S. Compos Part A – Appl S 2006, 37, 868.
10. Chen, B.; Chou, T. W. Compos Sci Technol 1999, 59, 1519.
11. Leclerc, J. S.; Ruiz, E. Compos Part A – Appl S 2008, 39, 1859.
12. Li, J.; Zhang, C.; Liang, R.; Wang, B.; Walsh, S. Polym Composite 2008, 29, 473.
13. Potter, K. Resin Transfer Moulding; Chapman & Hall: London, 1997.
14. Demaría, C.; Ruiz, E.; Trochu, F. Polym Composite 2007, 28, 797.
15. Schmachtenberg, E.; Heide, J. S. Z.; Topker, J. Polym Test 2005, 24, 330.
16. Stöven, T.; Weyrauch, F.; Mitschang, P.; Neitael, M. Compos Part A – Appl S 2003, 34, 475.
17. Lim, S. T.; Lee, W. I. Compos Sci Technol 2000.
18. Antonucci, V.; Giordano, M.; Nicolais, L.; Vita, G. D. Polym Eng Sci 2000, 40, 2471.
19. Prabhakaran, R. T. D.; Babu, B. J. C.; Agrawal, V. P. Polym Composite 2006, 27, 329.
20. Turner, D. Z.; Nakshatrala, K. B.; Hjelmstad, K. D. Polym Composite 2006, 27, 65.
21. Lee, Y. J.; Wu, J. H.; Hsu, Y.; Chung, C. H. Polym Composite 2006, 27, 665.
22. Advani, S. G.; Sozer, E. M. Process Modeling in Composites Manufacturing; Marcel Dekker: New York, 2002.
23. Cho, Y. K.; Song, Y. S.; Kang, T. J.; Chung, K.; Youn, J. R. Fiber Polym 2003, 4, 135.
24. Seong, D. G.; Chung, K.; Kang, T. J.; Youn, J. R. Polym Polym Compos 2002, 10, 493.
25. Song, Y. S.; Chung, K.; Kang, T. J.; Youn, J. R. Compos Sci Technol 2004, 64, 1629.
26. Lawrence, J. M.; Frey, P.; Obaid, A. A.; Yarlagadda, S.; Advani, S. G. Polym Composite 2007, 28, 442.
27. Chae, H. S.; Song, Y. S.; Youn, J. R. Korea-Aust Rheol J 2007, 19, 17.
28. Hattabi, M.; Echaabi, J.; Bensalah, M. O. Korea-Aust Rheol J 2008, 20, 7.
29. Binetruy, C.; Pabiot, J.; Hilaire, B. Polym Composite 2000, 21, 548.
30. Lin, M.; Hahn, H. T.; Huh, H. Compos Part A – Appl S 1998, 29, 541.
31. Béchet, E.; Ruiz, E.; Trochu, F. Compos Part A – Appl S 2003, 34, 813.
32. Trochu, F.; Gauvin, R.; Gao, D. M. Adv Polym Technol 1993, 12, 329.
33. Soukane, S.; Trochu, F. J Reinf Plast Comp 2005, 24, 1629.
34. Kang, M. K.; Lee, W. I. Compos Sci Technol 1999, 59, 1663.
35. Song, Y. S. Polym Composite 2007, 28, 458.
36. Shin, K. S.; Song, Y. S.; Youn, J. R. Korea-Aust Rheol J 2006, 18, 217.
37. Song, Y. S.; Chung, K.; Kang, T. J.; Youn, J. R. Polym Polym Compos 2003, 11, 465.
38. Lee, W.; Kim, J. H.; Shin, H. J.; Chung, K.; Kang, T. J.; Youn, J. R. Fiber Polym 2003, 4, 77.
39. Song, Y. S.; Chung, K.; Kang, T. J.; Youn, J. R. Polym Polym Compos 2005, 13, 323.
40. Song, Y. S.; Youn, J. R. Compos Part A – Appl S 2006, 37, 2080.